Nucleon polarization and cross section in photodisintegration of aligned and polarized deuterons at low and medium energies

Y. F. Zhang and M. L. Rustgi*
Department of Physics, State University of New York at Buffalo, Buffalo, New York 14260
(Received 3 August 1992; revised manuscript received 30 June 1993)

Effects of polarization and alignment of the deuteron on the polarization and cross section of the outgoing nucleons in deuteron photodisintegration have been investigated for low- and medium-energy gamma rays. Meson exchange currents and relativistic effects are included and the numerical calculations for the Paris potential are carried out. A comparison with the published results of Arenhövel and Schmitt is made.

PACS number(s): 24.70.+s, 25.10.+s, 25.20.−x

I. INTRODUCTION

The problem of the photodisintegration of the deuteron has been under investigation [1,2] since 1935. The importance of this process and its inverse at very low energies was emphasized, when it was shown by Riska and Brown [3] that the long standing 10% discrepancy between theoretical estimates and experimental measurements of the total cross section for radiative capture was compelling evidence for meson exchange current effects. The discrepancy between measurements [4] and calculations [5–7] for the 0° cross section led to the incorporation of relativistic corrections to the one- and two-body charge densities [8] and corrections due to the spin-orbit dipole operator [9]. However, the data continue to challenge the theory at low energies even when two-body charge and current effects are included [10–16].

Further information regarding both the electromagnetic and nuclear interactions of the deuteron may be obtained by studying the photodisintegration reaction from deuterons which are in a state of polarization and alignment. As early as 1961, Zickendraht, Andrews, and Rustgi (ZAR) [17] pointed out that the tests of the theories of photodisintegration can be extended by employing aligned and polarized deuterons. Employing the amplitude method [18], ZAR reported that the effects of alignment and polarization on the cross sections are quite pronounced. The results for cross section and polarization of photoprotons resulting from six different orientations of the deuteron by unpolarized gamma rays and including all electromagnetic multipoles up to $E4$ and $M4$ had been presented by Rustgi, Nunemaker, and Vyas [19]. The effect of the meson exchange currents and relativistic corrections to the one- and two-body charge densities were not considered in Refs. [17] and [19]. The object of this paper is to present results of such a study. The numerical results have been carried out for the Paris [20] potential. It is found that the effects of deuteron polarization are pronounced and increase with energy as electric dipole transitions predominate. At higher γ-ray energies (20–140 MeV) and also at 4.5 MeV, such studies have been made by Schmitt and Arenhövel [21–23]. A comparison with their results is made here.

*Deceased.

II. CALCULATIONS

The coordinate system used for the present calculation is shown in Fig. 1. The direction of the incident γ ray coincides with the positive z axis of a Cartesian coordinate system K with electric vector along the x axis. The quantization axis of the deuteron, denoted by $\mathbf{K}''$, is taken along the direction defined by the external field. The z' axis of another coordinate system K' is defined by the direction of the outgoing proton, the direction cosines of the x', y', and z' axis are $(\cos\theta\cos\phi, \cos\theta\sin\phi, -\sin\theta)$, $(-\sin\phi, \cos\phi, 0)$, and $(\sin\theta\cos\phi, \sin\theta\sin\phi, \cos\theta)$, respectively.

Following the notation and convention of Ref. [18], the interacting Hamiltonian for the traditional $E1$, $E2$, and $M1$ electromagnetic multipoles, on incorporating the relativistic one-body and the two-body charge density effects and the two-body current densities, may be written as

$$H' = -eE_x A \ , \tag{1}$$

where

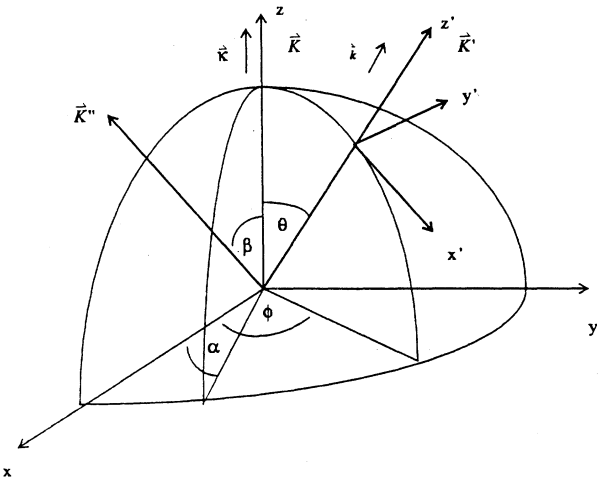

FIG. 1. Coordinate systems used. The plane polarized γ ray is incident along the positive z axis with the electric vector along the x axis. The polarization of the deuteron defines the $\mathbf{K}''$ axis and the outgoing proton defines the z' axis.

$$
\begin{aligned}
A=&\frac{1}{2}(\mathbf{1}_E\cdot\mathbf{r})+\frac{i}{8}(\mathbf{k}\cdot\mathbf{r})(\mathbf{1}_E\cdot\mathbf{r})\\
&+\frac{f^2}{4m}\{\tfrac{1}{3}(\phi_0\sigma_1\cdot\sigma_2+\phi_2\mathbf{S}_{12})\cdot\hat{\mathbf{r}}+(2\alpha_v\phi-\phi_1)[\sigma_1(\sigma_2\cdot\hat{\mathbf{r}})+\sigma_2(\sigma_1\cdot\hat{\mathbf{r}})]\}\cdot\mathbf{1}_E+\frac{3}{2}\frac{f^2}{M}\phi\alpha_s[\sigma_1(\hat{\mathbf{r}}\cdot\sigma_2)-\sigma_2(\hat{\mathbf{r}}\cdot\sigma_1)]\cdot\mathbf{1}_E\\
&+\frac{f^2}{2M}\frac{1}{\mu}\{\Phi_0[(\sigma_2\cdot\overleftrightarrow{\nabla})(\sigma_1\cdot\hat{\mathbf{r}})+(\sigma_1\cdot\overleftrightarrow{\nabla})(\sigma_2\cdot\hat{\mathbf{r}})]\hat{\mathbf{r}}+\frac{1}{3}[(3\Phi_1+\Phi_2)\sigma_1\cdot\sigma_2+\Phi_2S_{12}]\cdot\overleftrightarrow{\nabla}\}\cdot\mathbf{1}_E\\
&-\frac{1}{8M^2}\{(2\mu_v-1)(\sigma_1+\sigma_2)+2(\mu_s+1)(\sigma_1-\sigma_2)\}\times\mathbf{P}_r\cdot\mathbf{1}_E\\
&+\frac{\hbar}{2Mc}[(\tfrac{1}{2}\mu_v+g_I+h_I)(\sigma_1-\sigma_2)-\tfrac{1}{2}(\mu_s-\tfrac{1}{2})(\sigma_1-\sigma_2)+(g_{II}+h_{II})T_{12}^{(-)}]\cdot\mathbf{1}_H\ . \qquad (2)
\end{aligned}
$$

The formulas for the amplitudes, S^{ξ}_{mi}, for a final triplet or singlet state, when the initial state is given by Eqs. (2.1)–(2.3) of Ref. [18], are detailed in Eqs. (18.1)–(18.12) of Ref. [18]. The subscripts i and m are described in Eqs. (2.1)–(2.3) and (9.1)–(9.4) of Ref. [18], respectively, with $i=1,2,3$ and $m=0,1,2,3$. The initial state is a combination of spin-angle functions that transform under rotations like the Cartesian components of a vector. However, if the initial and final states are expressed in the usual spin-angle functions, the elements of the transition matrix S_{jk}, with $j=1,0,-1$ and $k=1,0,-1$ for triplet and s_{0k} for singlet states, can be obtained easily from S^{ξ}_{mi} by the inverse of Eqs. (2.1)–(2.3) and (9.1)–(9.4).

Replacing S_{ji} and s_{0i} on the right side of Eqs. (9.1)–(9.4) of Ref. [18] by S'_{ji} and s'_{0i}, their inverse transformation gives

$$
\begin{aligned}
&s'_{0i}=s^{\xi}_{\tilde{0}i}\ ,\\
&S'_{1i}=-\frac{1}{\sqrt{2}}(S^{\xi}_{1i}-iS^{\xi}_{2i})\ ,\\
&S'_{-1i}=\frac{1}{\sqrt{2}}(S^{\xi}_{1i}+iS^{\xi}_{2i})\ ,\\
&S'_{0i}=S^{\xi}_{3i}\ .
\end{aligned}
\qquad (3)
$$

Similarly from Ref. [18], the inverse transformation of Eqs. (2.1)–(2.3) gives S_{jk} as

$$
\begin{aligned}
&S_{j1}=-\frac{1}{\sqrt{2}}(S'_{j1}+iS'_{j2})\ ,\\
&S_{j0}=S'_{j3}\ ,\\
&S_{j-1}=\frac{1}{\sqrt{2}}(S'_{j1}-iS'_{j2})\ .
\end{aligned}
\qquad (4)
$$

The same transformation applies between s_{0i} and s'_{0i}. Combining these two transformations together and replacing s_{0i} by $S_{\tilde{0}i}$, the elements of the transition matrix from the initial state k to the final triplet or singlet state j, may be written as

$$
\begin{aligned}
&S_{\tilde{0}1}=-\frac{1}{\sqrt{2}}(S^{\xi}_{\tilde{0}1}+iS^{\xi}_{\tilde{0}2})\ ,\\
&S_{\tilde{0}0}=S^{\xi}_{\tilde{0}3}\ ,\\
&S_{\tilde{0}-1}=\frac{1}{\sqrt{2}}(S^{\xi}_{\tilde{0}1}-iS^{\xi}_{\tilde{0}2})\ ,
\end{aligned}
$$

$$
\begin{aligned}
&S_{11}=\frac{1}{2}[S^{\xi}_{11}+S^{\xi}_{22}+i(S^{\xi}_{12}-iS^{\xi}_{21})]\ ,\\
&S_{10}=-\frac{1}{\sqrt{2}}(S^{\xi}_{13}-iS^{\xi}_{23})\ ,\\
&S_{1-1}=-\frac{1}{2}[S^{\xi}_{11}-S^{\xi}_{22}-i(S^{\xi}_{12}+S^{\xi}_{21})]\ ,\\
&S_{01}=-\frac{1}{\sqrt{2}}(S^{\xi}_{31}+iS^{\xi}_{32})\ ,\\
&S_{00}=S^{\xi}_{33}\ ,\\
&S_{0-1}=\frac{1}{\sqrt{2}}(S^{\xi}_{31}-iS^{\xi}_{32})\ ,\\
&S_{-11}=-\frac{1}{2}[S^{\xi}_{11}-S^{\xi}_{22}+i(S^{\xi}_{12}+S^{\xi}_{21})]\ ,\\
&S_{-10}=\frac{1}{\sqrt{2}}(S^{\xi}_{13}+iS^{\xi}_{23})\ ,\\
&S_{-1-1}=\frac{1}{2}[S^{\xi}_{11}+S^{\xi}_{22}-i(S^{\xi}_{12}-S^{\xi}_{21})]\ .
\end{aligned}
\qquad (5)
$$

Equation (16.2) in Ref. [18] must be taken into account in calculation of S_{jk} if the γ rays are unpolarized.

In the cases of interest, the deuterons will be polarized and aligned by magnetic fields exterior to them. Then ρ_d, the density matrix of the deuteron, may be diagonalized by choosing the quantization axis of the deuteron, hereafter denoted by $\mathbf{K}''$ (see Fig. 1). Thus if the spin part of the deuteron state function is written as

$$\Psi^s_d=a_1\chi_1+a_0\chi_0+a_{-1}\chi_{-1}\ , \qquad (6)$$

where the χ_m are the usual spin 1 functions, the density matrix ρ_d may be written as

$$\rho_d=(I+\langle T_{10}\rangle T^{\dagger}_{10}+\langle T_{20}\rangle T^{\dagger}_{20})\ , \qquad (7)$$

where

$$\langle\mathbf{T}_{10}\rangle=\sqrt{\tfrac{3}{2}}(|a_1|^2-|a_{-1}|^2)=\sqrt{\tfrac{3}{2}}P_1\ , \qquad (8)$$

$$\langle\mathbf{T}_{20}\rangle=\frac{1}{\sqrt{2}}[3(|a_1|^2+|a_{-1}|^2)-2]=\frac{1}{\sqrt{2}}P_2\ , \qquad (9)$$

and P_1 is the polarization parameter, while P_2 is the alignment parameter specified in the notation of Blin-Stoyle and Grace [23]. The ranges of P_1 and P_2 are

$$-1\le P_1\le 1,\quad -2\le P_2\le 1\ .$$

The largest value of P_1 attainable with $P_2=0$ is $P_1=\frac{2}{3}$ corresponding to $|a_1|^2=\frac{2}{3}$, $|a_0|^2=\frac{1}{3}$.

If $\mathbf{K}''$ is rotated through angle (β,α) as shown in Fig. 1 then, since

$$\mathbf{T}_{jm}(\mathbf{K}'')=\sum_{m'} d_{m'm}(\alpha,\beta,0)\mathbf{T}_{jm'}(\mathbf{K}) , \tag{10}$$

the elements of ρ_d, after a little algebra, become

$$\begin{aligned}
\rho_{d_{11}}&=\frac{1}{3}+\frac{1}{2}P_1\cos\beta+\frac{1}{12}P_2(2-3\sin^2\beta) ,\\
\rho_{d_{12}}&=\left[\frac{1}{2\sqrt{2}}P_1\sin\beta+\frac{1}{2\sqrt{2}}P_2\sin\beta\cos\beta\right]e^{-i\alpha} ,\\
\rho_{d_{13}}&=\frac{1}{4}P_2\sin^2\beta e^{-i2\alpha} ,\\
\rho_{d_{21}}&=\left[\frac{1}{2\sqrt{2}}P_1\sin\beta+\frac{1}{2\sqrt{2}}P_2\sin\beta\cos\beta\right]e^{i\alpha} ,\\
\rho_{d_{22}}&=\frac{1}{3}-\frac{1}{6}P_2(2-3\sin^2\beta) ,\\
\rho_{d_{23}}&=\left[\frac{1}{2\sqrt{2}}P_1\sin\beta-\frac{1}{2\sqrt{2}}P_2\sin\beta\cos\beta\right]e^{-i\alpha} ,\\
\rho_{d_{31}}&=\frac{1}{4}P_2\sin^2\beta e^{i2\alpha} ,\\
\rho_{d_{32}}&=\left[\frac{1}{2\sqrt{2}}P_1\sin\beta-\frac{1}{2\sqrt{2}}P_2\sin\beta\cos\beta\right]e^{i\alpha} ,\\
\rho_{d_{33}}&=\frac{1}{3}-\frac{1}{2}P_1\cos\beta+\frac{1}{12}P_2(2-3\sin^2\beta) ,
\end{aligned} \tag{11}$$

where β and α are the colatitude and azimuthal angles that specify the orientation axis, $\mathbf{K}''$, of deuteron.

The differential cross section σ is then given by

$$\sigma=c(k)\bar{\sigma} , \tag{12}$$

where $c(k)=2\omega e^2/\hbar c\nu$ [see Eqs. (8) and (8.3) in Ref. [18]] and $\bar{\sigma}=\mathrm{Tr}(S\rho_d S^\dagger)$.

The polarization P of the ejected nucleon referred to the primed system defined in Fig. 1 is given by

$$P_i=c(k)\mathrm{Tr}[O_i(S\rho_d S^\dagger)]/\sigma , \tag{13}$$

where the observable O consists of products of the unit matrix and the proton and neutron spin operators so that a 4×4 representation of the latter is needed which may be obtained from Eqs. (6.1), (6.2), and (6.3) of Ref. [18].

For the proton they are

$$O_x=\frac{1}{\sqrt{2}}\begin{bmatrix}0&-1&0&1\\-1&0&1&0\\0&1&0&1\\1&0&1&0\end{bmatrix} ,$$

$$O_y=\frac{1}{\sqrt{2}}i\begin{bmatrix}0&-1&0&-1\\1&0&-1&0\\0&1&0&-1\\1&0&1&0\end{bmatrix} ,$$

$$O_z=\begin{bmatrix}0&0&1&0\\0&1&0&0\\1&0&0&0\\0&0&0&-1\end{bmatrix} ,$$

while for the neutron

$$O_x=\frac{1}{\sqrt{2}}\begin{bmatrix}0&1&0&-1\\1&0&1&0\\0&1&0&1\\-1&0&1&0\end{bmatrix} ,$$

$$O_y=\frac{1}{\sqrt{2}}i\begin{bmatrix}0&1&0&1\\-1&0&-1&0\\0&1&0&-1\\-1&0&1&0\end{bmatrix} , \tag{14}$$

$$O_z=\begin{bmatrix}0&0&-1&0\\0&1&0&0\\-1&0&0&0\\0&0&0&-1\end{bmatrix} .$$

III. RESULTS AND DISCUSSION

The amplitudes derived above were used to obtain expressions for the cross section and polarization of the ejected nucleon. The results of our calculation for the cross section $\sigma^{(p)}$ for the outgoing proton can be expressed in the form

$$\begin{aligned}
\sigma^{(p)}=&a+bC+cS^2+dS^2C+eS^2C^2+P_2\{[f+gC+hS^2+iS^2C+jS^2C^2+kS^4C+lS^4C^2](2-3\sin^2\beta)\\
&+S^2[m+nC+oC^2+pS^2C+qS^2C^2]\cos[2(\alpha-\phi)]\sin^2\beta\\
&+S[r+sC+tS^2+uS^2C+vS^2C^2+wS^4C]\cos(\alpha-\phi)\sin\beta\cos\beta\}\\
&+P_1\{S[x+yC+zS^2+z'S^2C]\sin(\alpha-\phi)\sin\beta\} ,
\end{aligned} \tag{15}$$

where $S=\sin\theta$, $C=\cos\theta$.

On making a comparison with the results of Ref. [23], it is found for cross section

$$\sigma^{(p)}=\frac{d\sigma_0}{d\Omega}\left\{P_1^{0,00}+P_2\left[\frac{1}{2}P_1^{0,20}(\theta)(2-3\sin^2\beta)-\frac{\sqrt{6}}{2}P_1^{0,21}(\theta)\cos(\alpha-\phi)\sin\beta\cos\beta+\frac{\sqrt{6}}{4}P_1^{0,22}(\theta)\cos2(\alpha-\phi)\sin^2\beta\right]\right.$$
$$\left.+P_1\left[-\frac{1}{\sqrt{2}}P_1^{0,11}(\theta)\sin(\alpha-\phi)\sin\beta\right]\right\},$$

where $d\sigma_0/d\Omega=a+bC+cS^2+dS^2C+eS^2C^2$ is the first five terms on the right-hand side of Eq. (15), while $P_1^{0,20}(\theta), P_1^{0,21}(\theta)$, etc. are the same as those given in Ref. [23].

The components of the polarization of the outgoing proton in the primed coordinate system are expressible in the form

$$P_{x'}^{(p)}\sigma^{(p)}=P_2\{S[a+bC+cS^2+dS^2C+eS^2C^2]\sin[2(\alpha-\phi)]\sin^2\beta$$
$$+[f+gC+hS^2+iS^2C+jS^2C^2+kS^4C]\sin(\alpha-\phi)\sin\beta\cos\beta\}$$
$$+P_1\{[l+mC+nS^2+oS^2C+pS^2C^2+qS^4C]\cos(\alpha-\phi)\sin\beta+S[r+sC+tS^2+uS^2C+vS^2C^2]\cos\beta\}$$
$$=\frac{d\sigma_0}{d\Omega}\left\{P_2\left[-\frac{\sqrt{6}}{2}P_x^{0,21}(\theta)\sin(\alpha-\phi)\sin\beta\cos\beta+\frac{\sqrt{6}}{4}P_x^{0,22}(\theta)\sin2(\alpha-\phi)\sin^2\beta\right]\right.$$
$$\left.+P_1\left[P_x^{0,10}(\theta)\cos\beta-\frac{1}{\sqrt{2}}P_x^{0,11}\cos(\alpha-\phi)\sin\beta\right]\right\}, \tag{16}$$

$$P_{y'}^{(p)}\sigma^{(p)}=S[a+bC+cS^2+dS^2C]+P_2\{S[e+fC+gS^2+hS^2C+iS^2C^2+jS^4C](2-3\sin^2\beta)$$
$$+S[k+lC+mS^2+nS^2C+oS^2C^2+pS^4C]\cos[2(\alpha-\phi)]\sin^2\beta$$
$$+[q+rC+sS^2+tS^2C+uS^2C^2+vS^4C+wS^4C^2]\cos(\alpha-\phi)\sin\beta\cos\beta\}$$
$$+P_1\{[x+yC+zS^2+z'S^2C+z''S^2C^2]\sin(\alpha-\phi)\sin\beta\}$$
$$=\frac{d\sigma_0}{d\Omega}\left\{P_y^{0,00}+P_2\left[\frac{1}{2}P_y^{0,20}(\theta)(2-3\sin^2\beta)-\frac{\sqrt{6}}{2}P_y^{0,21}(\theta)\cos(\alpha-\phi)\sin\beta\cos\beta\right.\right.$$
$$\left.\left.+\frac{\sqrt{6}}{4}P_y^{0,22}(\theta)\cos2(\alpha-\phi)\sin^2\beta\right]+P_1\left[-\frac{1}{\sqrt{2}}P_y^{0,11}(\theta)\sin(\alpha-\phi)\sin\beta\right]\right\}, \tag{17}$$

$$P_{z'}^{(p)}\sigma^{(p)}=P_2\{S^2[a+bC+cC^2+dS^2C]\sin[2(\alpha-\phi)]\sin^2\beta+S[e+fC+gS^2+hS^2C+iS^2C^2]\sin(\alpha-\phi)\sin\beta\cos\beta\}$$
$$+P_1\{S[j+kC+lS^2+mS^2C+nS^2C^2]\cos(\alpha-\phi)\sin\beta+[o+pC+qS^2+rS^2C+sS^2C^2+tS^4C]\cos\beta\}$$
$$=\frac{d\sigma_0}{d\Omega}\left\{P_2\left[-\frac{\sqrt{6}}{2}P_z^{0,21}(\theta)\sin(\alpha-\phi)\sin\beta\cos\beta+\frac{\sqrt{6}}{4}P_z^{0,22}(\theta)\sin2(\alpha-\phi)\sin^2\beta\right]\right.$$
$$\left.+P_1\left[P_z^{0,10}(\theta)\cos\beta-\frac{1}{\sqrt{2}}P_z^{0,11}\cos(\alpha-\phi)\sin\beta\right]\right\}. \tag{18}$$

The cross section and components of polarization of the outgoing neutron, $\sigma^{(n)}$, $P_{x'}^{(n)}$, $P_{y'}^{(n)}$, and $P_{z'}^{(n)}$, have the same form as $\sigma^{(p)}$, $P_{x'}^{(p)}$, $P_{y'}^{(p)}$, and $P_{z'}^{(p)}$ respectively, but the coefficients a, b, etc., are different. The following relation between $\sigma^{(p)}$ and $\sigma^{(n)}$ is always true:

$$\sigma^{(p)}(\theta,\phi,P_1,P_2,\beta,\alpha)=\sigma^{(n)}(\pi-\theta,\phi+\pi,P_1,P_2,\beta,\alpha)\ .$$

It is clear from Eqs. (15)–(18) that the parameters P_1 and P_2 of deuteron affect the differential cross section and polarization of the outgoing nucleon.

It is interesting to point out that for three mutually perpendicular aligned deuterons, in the directions (β,α), $(\beta+\pi/2,\alpha)$ and $(\pi/2,\alpha+\pi/2)$, the following relation, which has not been presented before [21–23], always holds:

$$\tfrac{1}{3}[F(\beta,\alpha)+F(\beta+\pi/2,\alpha)+F(\pi/2,\alpha+\pi/2)]_{0,P_2}=F_{0,0}\ , \tag{19}$$

where F may represent any of the quantities $\sigma^{(p)}$, $P_{x'}^{(p)}\sigma^{(p)}$, $P_{y'}^{(p)}\sigma^{(p)}$, $P_{z'}^{(p)}\sigma^{(p)}$, $\sigma^{(n)}$, $P_{x'}^{(n)}\sigma^{(n)}$, $P_{y'}^{(n)}\sigma^{(n)}$, and $P_{z'}^{(n)}\sigma^{(n)}$. The subscripts 0,0 indicate that $P_1=0$ and $P_2=0$.

Equation (15) gives for the total cross section

TABLE I. Values of σ_{t1}, σ_{t2} and their ratios at three γ-ray energies using the traditional interacting Hamiltonian. The values on including exchange current and relativistic corrections are given in parentheses.

E_γ (MeV)	σ_{t1} (μb)	σ_{t2} (μb)	σ_{t2}/σ_{t1}
22.2	479.4	−16.8	−0.0350
	(496.0)	(−13.2)	(−0.0266)
32.2	283.4	−12.3	−0.0433
	(296.9)	(−8.93)	(−0.0301)
62.2	111.8	−5.53	−0.0494
	(119.3)	(−3.16)	(−0.0265)

$$\sigma_t = 4\pi a + \frac{8\pi}{3}c + \frac{8\pi}{15}e + \left[4\pi f + \frac{8\pi}{3}h + \frac{8\pi}{15}j + \frac{32\pi}{105}l\right](2-3\sin^2\beta)P_2 = \sigma_{t1} + \sigma_{t2}(2-3\sin^2\beta)P_2 \quad (20)$$

where

$$\sigma_{t1} = 4\pi a + \frac{8\pi}{3}c + \frac{8\pi}{15}e \ , \quad (21)$$

$$\sigma_{t2} = 4\pi f + \frac{8\pi}{3}h + \frac{8\pi}{15}j + \frac{32\pi}{105}l \ . \quad (22)$$

Since $-2 \le (3\sin^2\beta - 2) \le 1$, and $-2 \le P_2 \le 1$, the orientation can affect σ_{t2} as much as the alignment does; the two together, affect σ_{t2} within a factor varying between -4 and 2. The effect of polarization, alignment, and orientation of the deuteron, on the total cross section has not been discussed before [21–23], and the numerical values are listed in Table I.

Figure 2 contains results for the proton polarization for an unpolarized γ ray of energy 10 MeV for different sets of values of $(\beta,\alpha,P_1,P_2,\phi)$. It is obvious from the figure that both the orientation and polarization of the deuteron can greatly affect the proton polarization. All three components of polarization reach their maximum around $\theta = 90°$, i.e., near the x-y plane. The component $P_{x'}^{(p)}$ reaches its maximum magnitude of 94.89% when the deuteron is completely polarized along the z axis and the proton is ejected in the x-z plane. The polarization component $P_{y'}^{(p)}$ reaches its maximum magnitude of 99.55% when the deuteron is completely polarized along the x axis and the proton is ejected in the y-z plane. The component $P_{z'}^{(p)}$ reaches its maximum magnitude of 98.06% when the deuteron is completely polarized along the x axis and the proton is ejected in the x-z plane. This indicates that the major contribution to the proton polarization comes from P_1, the polarization parameter of the deuteron. When the deuteron is partially polarized, $P_1 = 2/3$, the magnitude of polarization of all three components drops down as shown by curves marked 2 in the figure. Actually, the major contribution to $P_{y'}^{(p)}$ around 90° arises from the term zS^2 in Eq. (17), while the major contribution to $\sigma^{(p)}$ comes from the term cS^2 in Eq. (15). Since $P_{y'}^{(p)}$ is evaluated by taking the ratio of Eq. (17) to Eq. (15), these two terms are mostly responsible for the high percentage of $P_{y'}^{(p)}$ throughout the angular range extending from 30° to 150° at 10 MeV. This is even true at 2.754 MeV, though the results are not shown here. The major contribution to $P_{x'}^{(p)}$ and $P_{z'}^{(p)}$ comes from the terms tS^3 and lS^3 in Eq. (16) and Eq. (18), respectively. This explains why the curve 1 in both $P_{x'}^{(p)}$ and $P_{z'}^{(p)}$ behaves like $\sin\theta$ around $\theta = 90°$. The term cS^2 occurs in the unpolarized part of the cross section [Eq. (15)], but the three terms zS^2, tS^3, and lS^3 mentioned above occur in the P_1 part of Eqs. (17), (16), and (18), respectively. Therefore, the percentage of the three components of polarization are significantly dependent upon the magnitude of P_1. It is interesting to note that all three terms, zS^2, tS^3, and lS^3, do not originate from the $E1$-$M1$ interference. They predominantly result from the $E1$-$E1$ interference as has been also pointed out in Refs. [21–23], though $E2$ and $M1$ transitions to triplet states also contribute a little for a 10 MeV γ ray. It is found that the $E2$ multipole contributes at most 3% to the polarization components, while the $M1$-to-triplet transitions account for less than 2%. In the flat part of $P_{y'}^{(p)}$ ($30° \le \theta \le 150°$), these two multipoles altogether do not contribute more than 1.4% to the polarization. This is even true at lower γ-ray ener-

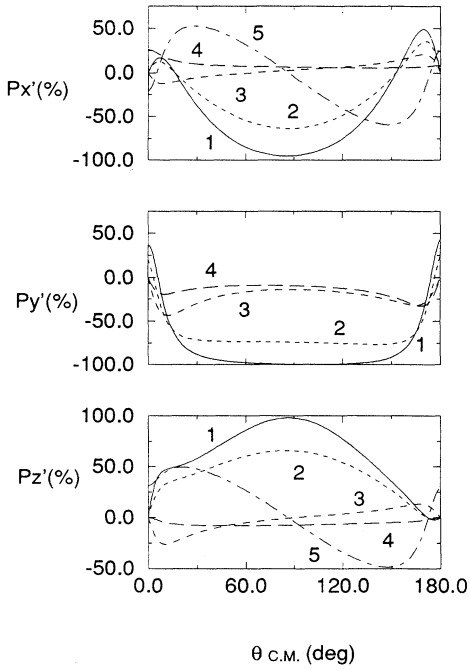

FIG. 2. The polarization of photoprotons resulting from disintegration of oriented deuterons by unpolarized photons of energy 10 MeV employing the Paris potential. The exchange current and relativistic correction are included. The curves are labeled by five parameters $(\beta,\alpha,P_1,P_2,\phi)$. For $P_{x'}$, curves 1–5 correspond to (0°,0°,1,1,0°), (0°,0°,2/3,0,0°), (90°,0°,0,1,45°), (45°,0°,0,1,90°), and (90°,0°,2/3,0,0°), respectively. For $P_{y'}$ curves 1–4 refer to (90°,0°,1,1,90°), (90°,0°,2/3,0,90°), (0°,0°,0,1,0°), and (0°,0°,0,0,0°); and for $P_{z'}$, curves 1–5 refer to (90°,0°,1,1,0°), (90°,0°,2/3,0,0°), (45°,0°,0,1,90°), (90°,0°,0,1,45°), and (0°,0°,2/3,0,0°).

gies of say 2.754 MeV. Hence, it becomes clear that the polarization of deuteron enhances the $E1$-$E1$ interference contribution, resulting in a high percentage of polarization of the outgoing proton.

At lower γ-ray energy of 2.754 MeV, not shown in the figure in the interest of brevity, the maximum percentage of proton polarization drops down to 80%, 89%, and 91% for the $P_{x'}^{(p)}$, $P_{y'}^{(p)}$, and $P_{z'}^{(p)}$ components, respectively. For $P_1=P_2=0$, $(\sigma^{(p)}P_{y'}^{(p)})$ consists entirely of singlet-triplet amplitude products, which results in a decrease of $P_{y'}^{(p)}=(\sigma^{(p)}P_{y'}^{(p)}/\sigma^{(p)}$ at $E_\gamma=2.754$ MeV due to a large increase of $\sigma^{(p)}$ arising from electric dipole transitions, which is not matched in the numerator. The increase of $\sigma^{(p)}P_{y'}^{(p)}$ due to deuteron polarization is overwhelmingly of triplet-triplet origin and matches the increase in $\sigma^{(p)}$. It is also found that the maximum polarization increases in magnitude from about 90% to almost 100%, as the γ-ray energy is increased from 2.754 to 10 MeV.

The pattern of polarization of the outgoing neutron is usually similar to that of the proton.

Three-dimensional graph helps visualize the spatial distribution directly. Figure 3 describes the spatial distribution of $P_{y'}^{(p)}$ for 62.2 MeV γ-ray energy, when the deuteron is aligned ($P_1=0$, $P_2=-2$) in the x direction. Both angles θ and ϕ can affect $P_{y'}^{(p)}$ significantly. $P_{y'}^{(p)}$ reaches its negative maximum of -76% when the proton is ejected in the direction ($\theta=137°$, $\phi=0°$, or 180°). However, $P_{y'}^{(p)}$ drops to a few percent if $\phi=90°$ or 270°. Figure 3(b) shows that exchange current and relativistic correction increase the magnitude of $P_{y'}^{(p)}$ considerably in this case.

Since α and ϕ always appear in the form $(\alpha-\phi)$ in equations (15), (16), (17), and (18), α affects the polarization and cross section in a way similar to ϕ when one of them is fixed and the other one is varied.

The variation of maximum magnitude of proton polarization as a function of energy is shown in Fig. 4. The magnitudes of $P_{y'}^{(p)}$ and $P_{z'}^{(p)}$ increase from about 90% to almost 100% as the γ-ray energy is increased from 2.754 to 10 MeV. They drop down to about 80% as the energy continues to increase to 62.2 MeV. The magnitude of $P_{x'}^{(p)}$ changes in a similar pattern, but covers an even wider range. All three magnitudes reach their maximum around $E_\gamma=10$ MeV, because $P_{x'}^{(p)}$, $P_{y'}^{(p)}$, and $P_{z'}^{(p)}$ are given by the ratio of Eqs. (16), (17), and (18) to Eq. (15) respectively. At low energy, both $E1$ and $M1$ to singlet transitions give important contribution to Eq. (15), while $E1$ transition predominates the contribution to the other three equations near the maximum, and up to about 20 MeV gamma-ray energy. Hence, the three ratios increase with E_γ in low-energy region since the contribution of the $M1$ transition drops down faster than $E1$ transition. The three ratios decrease with E_γ in higher-energy region when $E2$-, and $M1$-to-triplet transitions play a more and

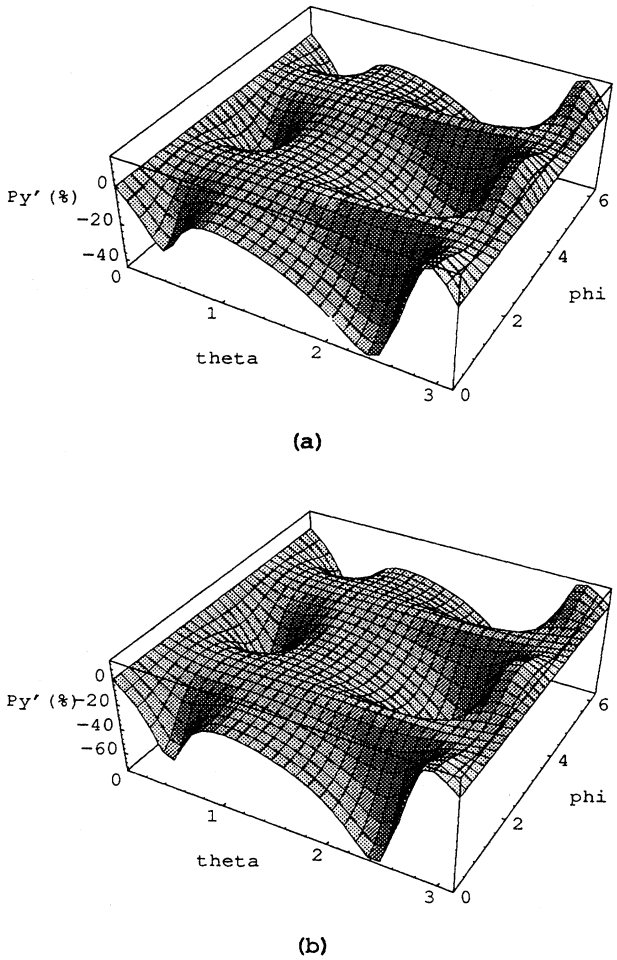

FIG. 3. Three-dimensional display of the y' component of proton polarization for $E_\gamma=62.2$ MeV. The angles θ and ϕ are in unit of radians.

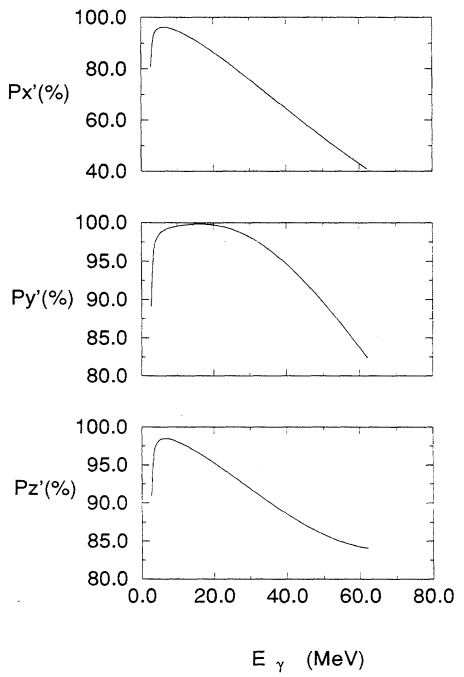

FIG. 4. Maximum (magnitude) polarization as a function of gamma-ray energy.

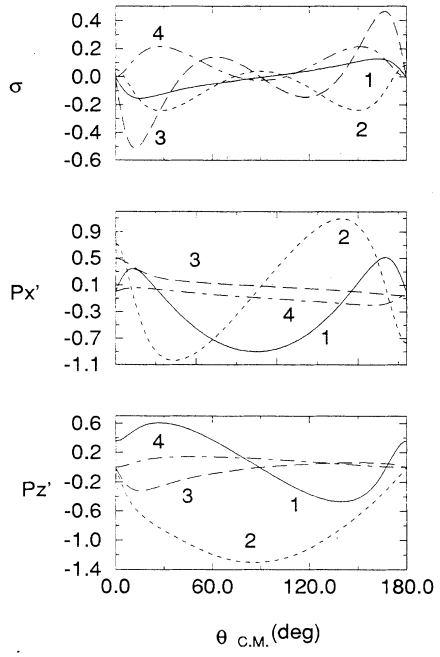

FIG. 5. Cross section and polarization for protons as a function of θ for 20 MeV incident γ ray. For cross section, curves 1, 2, 3, and 4 correspond to $P_1^{0,11}$, $P_1^{0,20}$, $P_1^{0,21}$, and $P_1^{0,22}$ while polarization components $P_x^{0,10}$, $P_x^{0,11}$, $P_x^{0,21}$, and $P_x^{0,22}$ are represented by curves 1, 2, 3, and 4, respectively. The same notation applies to the z' components of polarization.

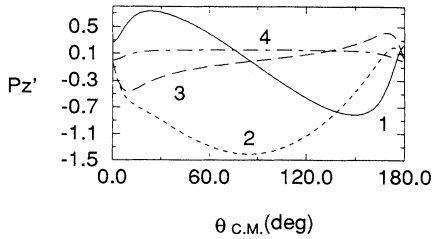

FIG. 6. Same as the z' component of polarization in Fig. 5, but the γ-ray energy is 4.5 MeV.

more important role.

Our results of polarization and cross section generally agree with those of Ref. [23]. For a detailed comparison, some of our results are plotted in Figs. 5 and 6. In making this comparison, the contribution of higher multipoles considered in Ref. [23] has been kept in mind [25]. The isobar configurations are not supposed to be significant at such low energies. Figure 5 shows various cross sections and polarization of the outgoing proton when the gamma-ray energy is 20 MeV. Most of our curves are similar to those given in Ref. [23]. But some differences are obvious, too. For example, the component $P_1^{0,20}$ (curve 2) of the cross section is positive in the forward and backward directions in our calculation but it is quite negative in Ref. [23], making the two curves quite different in shape. More differences can be seen in the x' component of polarization. The magnitude of our $P_x^{0,11}$ (curve 2) exceeds 1, while the corresponding one in Ref. [23] is always less than 1, though the two curves are similar in shape. For $P_x^{0,22}$, our magnitude in the backward region (150°–180°) is much less than given in Ref. [23]. Also, there is some difference between shapes of the curves for $P_x^{0,21}$ (curve 3). Like $P_x^{0,11}$, the magnitude of our $P_z^{0,11}$ (curve 2) is also bigger than the corresponding one in Ref. [23]. Our value of $P_z^{0,11}$ reaches a value as low as -1.3, while in Ref. [23] it is around -1. Besides, our $P_z^{0,10}$ (curve 1) appears to be more positive than that given in Ref. [23].

At lower gamma-ray energy of 4.5 MeV, our results become closer to those in Ref. [23] except for the curve of $P_z^{0,11}$ (curve 2). The magnitude of our $P_z^{0,11}$ reaches 1.4 as shown in Fig. 6, while in Ref. [23] it has a maximum value of 1.1. These differences [Figs. 5 and 6] take added importance because they occur at such low energies.

In the present paper we have studied the polarization and cross section of the outgoing nucleons employing polarized and aligned deuterons for low- and medium-energy gamma rays. Though in the energy region investigated our results generally agree with those of Arenhövel and Schmitt, some significant differences are found. It is found that for polarized deuterons, up to about 20 MeV, almost the entire nucleon polarization is produced by the $E1$ interaction in contrast to the $E1$-$M1$ interference term which is responsible for nucleon polarization when unpolarized deuterons are used. It is hoped that through this investigation enough experimental interest may be stimulated in the measurement of such large polarization for the theoretical analysis is more secure in this low-energy region.

At present aligned and polarized deuteron sources are being prepared at various laboratories. These results will also help guide the experimentalists in the planning of their experiments.

[1] J. Chadwick and M. Goldhaber, Nature **134**, 237 (1934).
[2] H. A. Bethe and R. Peierls, Proc. R. Soc. **A148**, 146 (1935).
[3] D. O. Riska and G. E. Brown, Phys. Lett. **38B**, 193 (1972).
[4] R. J. Hughes, A. Ziegler, H. Waffler, and B. Ziegler, Nucl. Phys. **A267**, 329 (1976).
[5] H. Arenhövel and W. Fabian, Nucl. Phys. **A282**, 397 (1977).
[6] E. L. Lomon, Phys. Lett. **68B**, 419 (1977).
[7] M. L. Rustgi, T. S. Sandhu, and O. P. Rustgi, Phys. Lett. **70B**, 145 (1977).
[8] A. Cambi, B. Mosconi, and P. Ricci, Phys. Rev. Lett. **48**, 462 (1982).
[9] J. L. Friar, B. F. Gibson, and G. L. Payne, Phys. Rev. C **30**, 441 (1984); **31**, 287(E) (1985).
[10] R. O. Jewell, W. John, J. E. Sherwood, and D. H. White, Phys. Rev. **139**, B71 (1965).
[11] R. J. Holt, K. Stevenson, and J. R. Specht, Phys. Rev.

Lett. **50**, 577 (1983).
[12] M. L. Rustgi, R. Vyas, and M. Chopra, Phys. Rev. Lett. **50**, 236 (1983).
[13] K. Stephenson, R. J. Holt, R. D. Mckeown, and J. R. Specht, Phys. Rev. C **35**, 2023 (1987).
[14] E. J. Hadjimichael, M. L. Rustigi, and L. N. Pandey, Phys. Rev. C **36**, 44 (1987).
[15] Y. Birenbaum, Z. Berant, A. Wolf, S. Kahane, and R. Moreh, Phys. Rev. Lett. **61**, 810 (1988).
[16] A. Kassaee, L. N. Pandey, M. L. Rustgi, and E. Hadjimichael, Phys. Rev. C **39**, 1147 (1989).
[17] W. Zickendraht, D. J. Andrews, and M. L. Rustgi, Phys. Rev. Lett. **7**, 252 (1961).
[18] M. L. Rustgi, W. Zernik, G. Breit, and D. J. Andrews, Phys. Rev. **120**, 1881 (1960); L. N. Pandey and M. L. Rustgi, Phys. Rev. C **32**, 1842 (1985). The notation and conventions used in these papers are followed here.
[19] M. L. Rustgi, R. D. Nunemaker, and R. Vyas, Can. J. Phys. **62**, 1064 (1984).
[20] M. Lacombe *et al.*, Phys. Rev. C **21**, 861 (1980).
[21] H. Arenhövel, Few-Body Systems **4**, 55 (1988).
[22] H. Arenhövel and K.-M. Schmitt, Few-Body Systems **8**, 7 (1990).
[23] K.-M. Schmitt and H. Arenhövel, Few-Body Systems **11**, 33 (1991); see also Few-Body Systems Suppl. **4** (1991).
[24] R. J. Blin-Stoyle and M. A. Grace, in *Handbuch der Physik*, edited by F. Flügge (Springer-Verlag, Berlin, 1957), Vol. 42, p. 555, especially pp. 557–559.
[25] M. L. Rustgi, L. N. Pandey, and A. Kassaee, Phys. Rev. C **33**, 1823 (1986).